Technology Milestone Whitepaper

Development of a Method for Exoplanet Imaging in Multi-Star Systems

Ruslan Belikov (PI), Eduardo Bendek (deputy PI), Dan Sirbu, Eugene Pluzhnik, Stephen Bryson
(NASA Ames Research Center)

Stuart Shaklan, A J Eldorado Riggs, Brian Kern, John Krist, John Trauger
(NASA Jet Propulsion Laboratory)

Tyler Groff
(NASA Goddard Space Flight Center)

Olivier Guyon
(Subaru Telescope)

Julien Lozi
(Research Corporation of the University of Hawaii / Subaru Telescope)

Sandrine Thomas
(Large Synoptic Survey Telescope)

Approvals

Released by

Ruslan Belikov — Date
Principal Investigator, NASA ARC

Approved by

Nicholas Siegler — Date
Exoplanet Exploration Program Chief Technologist, NASA JPL

E-SIGNED by Brendan Crill
on 2018-02-09 02:32:08 GMT

Brendan Crill — Date
Exoplanet Exploration Deputy Program Chief Technologist, NASA JPL

Douglas Hudgins — Date
Exoplanet Exploration Program Scientist, NASA-HQ

Contents

1 Objective

The objective of this work is to continue to mature a technique called "Multi-Star Wavefront Control" (MSWC) from TRL3 to 4. MSWC enables the capability to directly image exoplanets and disks in multi-star systems, including important nearby targets such as Alpha Centauri (αCen), with existing direct imaging mission concepts. MSWC is a wavefront control algorithm that in principle does not require any hardware modifications to any internal coronagraph or external occulter mission concept as long as a DM is present. The specific objectives of this work are to:

- Develop a MSWC algorithm and validate its model against laboratory experiments
- Show with validated models that MSWC can achieve performance on binary targets that is similar to the single-star performance on missions such as WFIRST, HabEx and LUVOIR [1].
- Demonstrate MSWC on a real instrument to ground-based level contrasts.
- Perform a high contrast laboratory demonstration of MSWC (down to the contrast levels the Ames Coronagraph Experiment laboratory is able to achieve)

These objectives are synergistic and interrelated with each other, and are realized by meeting a milestone that is associated with each of them, as described in section 3. Together they fully prepare MSWC for TRL5+ vacuum testing.

2 Introduction / Background

2.1 Motivation

2.1.1 Mission Concepts benefited by this technology

All the internal coronagraph missions to directly image exoplanets involve a starlight suppression instrument whose relevant elements are shown in Figure 1. Great strides have been made to mature internal coronagraphs for single star systems, but not yet for multi-star systems. The MSWC method that we proposed to develop here uses the existing wavefront control system shown in blue on Figure 1 to enable direct imaging of exoplanets in multi-star systems. In principle, no new modifications or new requirements are necessary on the telescope, though minor hardware modifications may improve performance as will be described later. For external occulter-based missions, the only hardware modification would be an inclusion of a DM on the telescope.

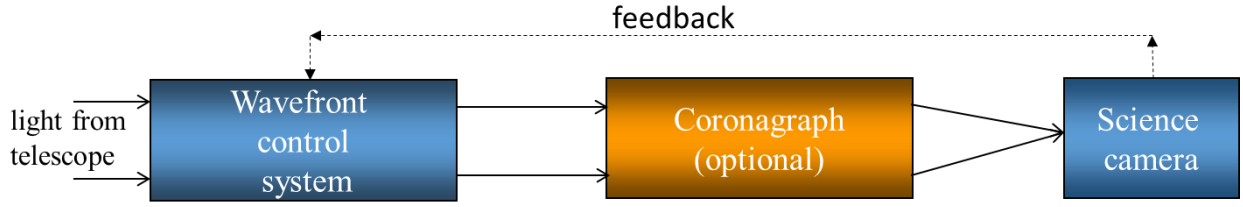

Figure 1. Diagram of a starlight suppression system for a direct imaging mission. Any mission containing the blue boxes can in principle make use of the methods proposed here. (Note: the coronagraph is sometimes upstream of the wavefront control system. For external occulter missions, a DM must be present on the telescope.)

Thus, in principle our technology benefits, and is compatible with, any direct imaging mission with no or minor modifications, as long as it contains a DM or an equivalent active optical device. With the work described here, we aim to advance MSWC specifically for the WFIRST, LUVOIR, and HabEx mission concepts, and enable those missions to directly image planets orbiting almost any nearby binary star (which would usually orbit in a circumstellar, rather than circumbinary fashion).

2.1.2 Science significance

The science promised by space-based high contrast imaging missions will result in great leaps in our understanding of warm disks, exoplanetary diversity, dynamics, and atmospheres, a census of exoplanets around nearby stars, and the detection and spectral characterization of Earth-like planets in the habitable zone. However, none of these missions can image multi-star systems with current technology except when the leak and glare of the companion star(s) is negligible or small enough to be removed by post-processing. Therefore, many systems with multiple stars (or optical multiples) are often excluded from target lists of such missions.

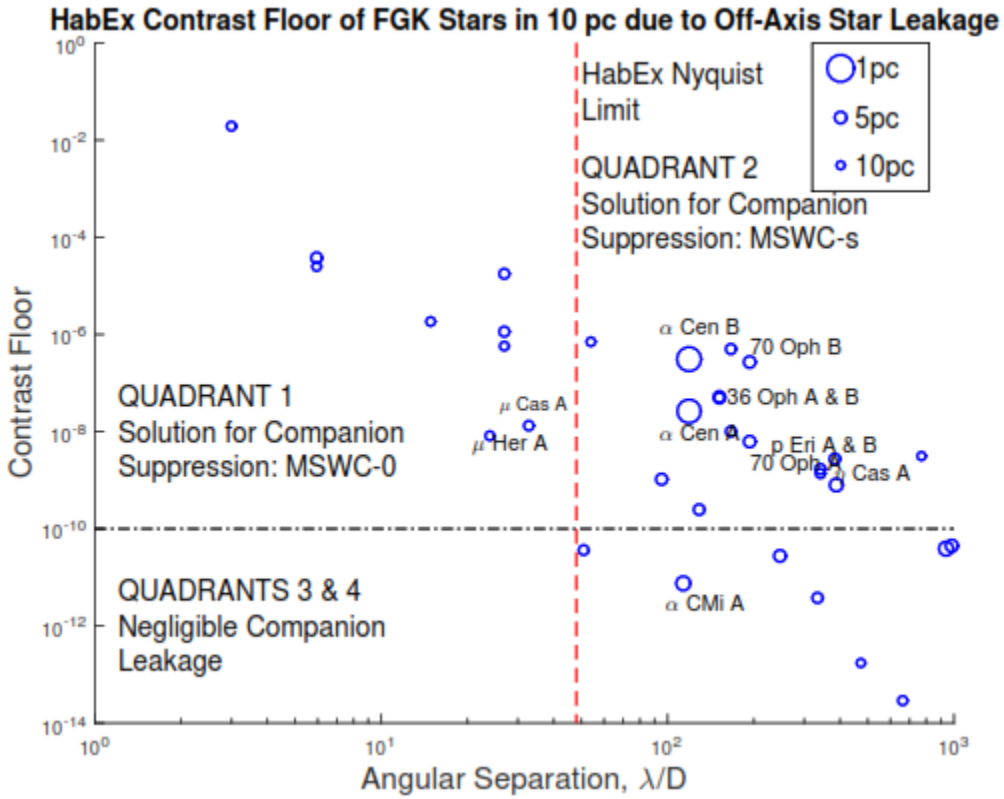

Figure 2. Multi-star systems within 10pc. The x-axis is the binary separation (at current epoch for a 4 m telescope and λ=650 nm) and the y-axis is the contamination suffered by the on-axis target star from an off-axis companion, due to diffraction and optical aberrations (λ/20 rms end-to-end wavefront error and a f^2 power spectral density). Values above ~10^{-10} compromise the ability to detect potentially habitable planets, but can be recovered with MSWC.

Enabling the study of multi-star systems is very important because the majority of K-type and earlier stars are in multi-star systems. For example, 5 out of the 7 star systems within 4 parsecs

containing K- or earlier type stars are multiple (α Cen, Sirius, Procyon, 61 Cyg, ε Ind), and only two are single (ε Eri, τ Cet). While it is true that there are many more nearby M-dwarfs and most of them are single, the direct imaging of M dwarfs is arguably better done from the ground with ELTs because: (a) they are dimmer and require larger apertures; (b) their planetary systems are closer to the star and require the angular resolution of larger apertures; (c) because planets are closer to the star, contrast is easier, so that the presence of the atmosphere is less serious. Conversely, the study of K- and earlier type stars arguably favors space-based missions, for which the smaller apertures are not as much of a concern, but which require much deeper contrasts only possible from space. Therefore, most of the stars best suited for space missions are in fact in multi-star systems and the methods proposed here promise to greatly increase the science yield of such missions, as well as enable the study of a whole new class of star systems, namely multiple stars.

The benefit to science yield can be quantified slightly better by assessing how many out of nearby FGK stars are multiples, and how many of those have a companion that leaks too much light into the other star's region of interest. A SIMBAD search reveals that there are 69 FGK stars within 10 pc of the Sun, out of which 42 (61%) have at least one companion. If we assume a 4m telescope (typical HabEx size) with λ/20 rms end-to-end wavefront error and a f^2 power spectral density, then 25 of the stars suffer more than 10^{-10} contrast contamination from the companion and 12 that suffer more than 10^{-7} (see Figure 2). Although the exact amount of contamination depends on many specific details (size of the aperture, type and amount of error, epoch, and location of region of interest), it is clear that MSWC will significantly increase the yield of planets, including Earth-like ones.

Table 1. Selected nearby binary star targets. Off-axis leakage is the contamination of the on-axis region of interest by light from an off-axis star, in units of contrast. Angular separation is computed for λ = 650nm and D = 4m.

Target Star	Spectral Type	Dist. (pc)	Vmag	Comp. Ang. Sep (arcsec)	Comp. Ang. Sep (λ/D)	Comp. ΔVmag	Off-Axis Leakage (Contrast Floor)
α Cen A	G2V	1.3	0.0	4.0	119.3	1.3	2.7e-08
α Cen B	K1V	1.3	1.3	4.0	119.3	-1.3	3.1e-07
70 Oph A	K0V	5.1	4.1	6.5	193.3	2.0	6.3e-09
70 Oph B	K4V	5.1	6.1	6.5	193.3	-2.0	2.7e-07
36 Oph A	K2V	5.5	5.1	5.1	152.2	0.0	4.8e-08
36 Oph B	K1V	5.5	5.1	5.1	152.2	0.0	5.2e-08
μ Cas A	K1V	7.6	5.2	1.1	32.8	5.4	1.3e-08
p Eri A	K2V	7.8	5.7	11.4	340.1	0.2	1.4e-09
p Eri B	K2V	7.8	5.9	11.4	340.1	-0.2	1.9e-09
μ Her A	G5IV	8.3	3.4	0.8	23.9	7.3	8.4e-09

2.1.3 Science highlight: α Centauri

The αCen system represents a particularly attractive target for direct imaging missions, except for the fact that it is a binary system. Aside from its multiplicity, the A and B stars of the system are unusually and fortunately low-hanging fruits that are 3 times easier than the next easiest target

by almost any metric (see Figure 3, left). In particular, the next closest star earlier than M-type (ε Eri) is 2.4 times as far, and is known to have a thick disk that may interfere with detection of small planets. The next star of comparable proximity to α Cen is Barnard's star, which is 1.4 times farther, has a much dimmer magnitude of 10, and has a habitable zone only 30mas wide, about 30x smaller than αCen. In fact, αCenA habitable zone spans such a large angle on the sky (~1") that it is outside the *outer* working angle of many large mission concepts. The planetary system around αCen would be imaged in at least ~3x higher spatial and spectral resolution (in the photon-noise limited regime) than around any other star, or have at least ~3x SNR for a given spectral resolution. Due to this fact, a mission not designed to directly image potentially habitable planets may nevertheless still be able to do this around Alpha Centauri (for example, WFIRST if it slightly outperforms its design requirements and if MSWC can be matured). A mission not designed to detect spectral biomarkers might still be capable of doing this around αCen.

The right side of Figure 3 shows that an Earth twin around α Cen A (or B) will be very obvious on a mission at least as large as Exo-C (1.5m aperture, [2]), if the companion star could be removed and if the exo-zodi level is similar to Solar. An Earth twin can even be theoretically imaged with a 0.25m (25cm) telescope in ~10 hours with a powerful enough coronagraph and wavefront control system [3,4]. Even at that extremely small aperture, an Earth twin will appear 2.7 λ/D away from the A star at maximum elongation, and have a flux of 1 photon per minute (after accounting for coronagraph and other throughput losses), which is typical of NASA's larger mission concepts imaging planets at 10pc. The potential existence of a brighter exo-zodi around α Cen (as tentatively suggested in [5]) may of course overwhelm the light of the exo-Earth. However, the unusual proximity of the target also ameliorates the effects of exo-zodi. Furthermore, if there is indeed an exo-zodi bright enough to overwhelm small planets, it will give us the best opportunity to study structural disk details in much higher definition than around any other star.

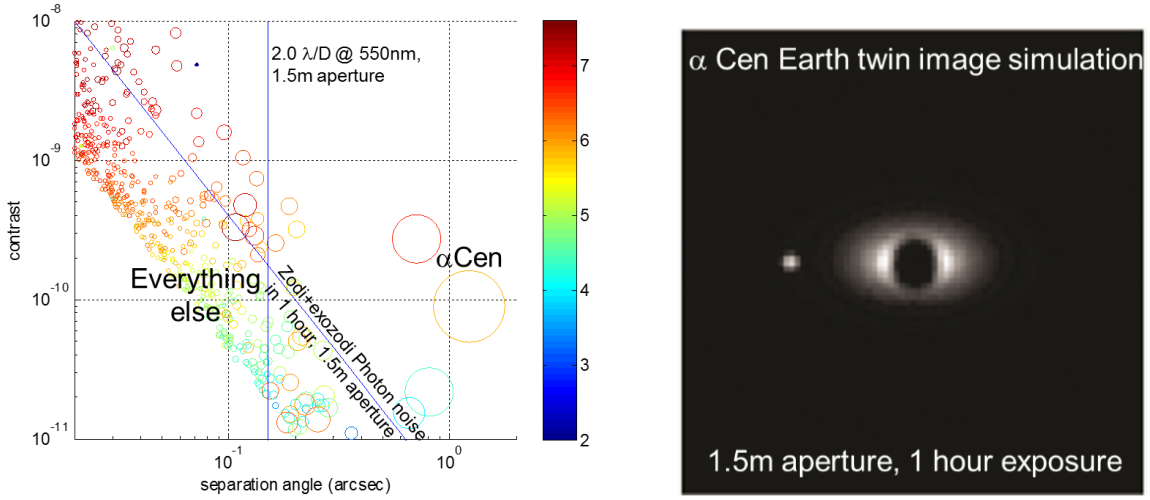

Figure 3. Left: Simulation of an Earth twin at maximum separation around every real nearby star. Circle size and color represent star size and type. Almost any mission would image planets around with at least ~3x higher spatial and spectral resolution than any other star, except for the fact that it is a binary. Right: Simulated image of an Earth twin around α Cen A for the PECO mission (similar to Exo-C). Among included effects were zodi, exozodi = 1 zodi, photon noise. Companion star was excluded.

In short, if α Cen was a single star, it would probably be on the top of the target list for any direct imaging mission, and (if it has potentially habitable planets) would probably end up being

the science highlight of any finished mission. But, it remains just out of reach, along with many other interesting binaries, because the technology to suppress binary starlight is not yet mature.

2.2 Background on Multi-Star Wavefront Control

We briefly summarize the theory behind MSWC, which is covered in more detail in recent publications [6,7]. Let us assume for the moment that a coronagraph or external occulter is completely removing all the light from the on-axis star in a binary system. What remains is then the off-axis star (typically at a super-Nyquist separation), and our job is to suppress the light of the off-axis star that leaks into the region of interest around the on-axis star. Two fundamentally different effects contribute to create this light leak: diffraction and optical aberrations. As a general rule, diffraction dominates close to the star but aberrations dominate far from the star (for typical mirror aberrations). The transition usually occurs on the order of 10 λ/D away from the star. All coronagraphs suppress diffraction, but they do not help with aberrations (except for pinned speckles). A wavefront control (WC) system, or at least some active optical element such as a deformable mirror, is required to suppress optical aberrations. In addition to suppressing aberrations, a deformable mirror is often capable of suppressing diffraction by at least an order of magnitude. Therefore, a second (off-axis) coronagraph is neither sufficient nor necessary to suppress the leak of the off-axis star, while a wavefront control system is both necessary and (almost always) sufficient to suppress both the aberrations and diffraction. This goes contrary to the "common wisdom" that the proper way to address the second star in a binary system is to design a coronagraph to block both stars. A coronagraph is only useful if the two stars have an uncommonly close separation (< ~10 λ/D) where light leak caused by diffraction of the off-axis star dominates. Of course, one can think of the deformable mirror acting as a "phase mask coronagraph" for the second star, in addition to suppressing aberrations.

Thus, our solution to binary star suppression, (MSWC) is a new wavefront control algorithm rather than a new binary coronagraph design. Wavefront control in binary stars poses two non-trivial challenges as compared to single stars, which we call "sub-Nyquist MSWC" (MSWC-0) and "Super-Nyquist MSWC" (MSWC-s). Sub-Nyquist refers to the case where the region of interest is within the conventional control radius of the DM (for example, 16 λ/D for a 32x32 DM) with respect to both stars. Super-Nyquist refers to regions outside the sub-Nyquist region.

2.2.1 Sub-Nyquist Multi-Star Wavefront Control: Theory

In general, any region of interest where we wish to detect planets contains a mix of speckles from both stars. The fundamental problem is that these two speckle fields are mutually incoherent. If conventional single-star wavefront control is applied, it will at best remove the speckles of one of the stars but not the other. If single star wavefront control is applied to sequentially to suppress speckles from star A, then from star B, that will disrupt the speckle suppression for star A. Thus, in order to suppress both stars, it is necessary to *independently* suppress the speckle fields of each star in the region of interest.

This turns out to be possible, if the region of interest is chosen properly. Figure 4 shows the special case of two stars separated by 16 λ/D, in a system like Figure 1 with a DM but no coronagraph (for simplicity). The stars are high Strehl, but do not look like Airy patterns to the eye because the brightness is stretched over 7 orders of magnitude. Also, the DM does not flatten out wavefront errors, but rather has a special MSWC-computed pattern. The dashed red square on the left panel is the (sub-Nyquist) control region of a 32x32 DM with respect to star A. This region

can be conceptually separated into 4 vertical sections, controlled by different sets of modes on the DM (the outer sections are controlled primarily by modes on the DM corresponding to spatial frequencies of 8-16 cycles per aperture (cpa), and the inner regions are controlled primarily by 0-8 cpa). The middle panel of Figure 4 shows the same situation, but with respect to star B (yellow color). Finally, the right panel superimposes these two images. One can define a region (outlined in white) where speckles from star A and star B are modulated by two completely disjoint sets of DM modes: 0-8 cpa for star A and 8-16 cpa for star B.

In the white region, the speckle field of the A star can be suppressed by using the 0-8 cpa modes without affecting the B star much and the speckle field of the B star can be independently suppressed by using the 8-16 cpa modes without affecting the A star much. In effect, we have reduced the MSWC problem to two separate conventional WC problems (each using different DM modes), which we know how to solve using any standard single-star WC algorithm. Solving these two conventional WC problems simultaneously results in simultaneous suppression of the speckle fields of both stars in the white region of interest. The same can be done in other region shapes, as long as DM modes from star A and star B do not overlap anywhere in the region of interest. We call such regions "non-redundant". Non-redundant regions can have many different shapes, but their area must be half of the area of a single-star control region, to conserve the number of degrees of freedom defined by the number of DM actuators. The final result is that a 2-star dark zone can be created anywhere within the sub-Nyquist limit of both stars, at the expense of reducing the size of the control region by a factor of two. To recover the larger area of a single-star control zone, two smaller regions can be suppressed separately and then stitched together to create the larger zone.

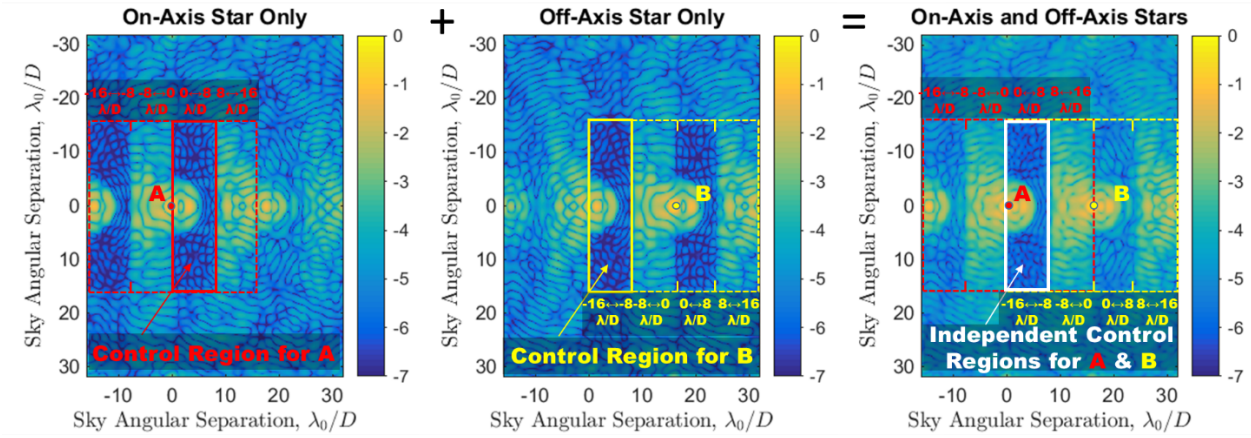

Figure 4. Basic principle behind MSWC: using different modes on one DM to independently modulate light for two different stars. The three panels show a simulation of a non-coronagraphic focal plane image with two stars and a MSWC-computed deformable mirror setting. Individual stars are shown only for clarity. In reality, only the combined image can be obtained. Nevertheless, MSWC is capable of estimating and correcting both speckle fields independently in the region of interest

MSWC also generalizes to N-star systems, but then the non-redundant regions of interest will have 1/N the area of a single-star region for a given DM. It turns out that these regions can always fully span the (sub-Nyquist) focal plane field if stitched together. This is related to the so-called Voronoi partitions.

It should be noted that in practice it is impossible to completely decouple DM modes – any DM mode will always affect all stars everywhere to some level. However, on the regions we

constructed, one of the star's speckle fields is affected much more than the other, so degeneracies are avoided almost everywhere.

Any mature focal plane-based single-star wavefront control algorithm can be generalized to MSWC. These include, for example, classical speckle nulling, stroke minimization [8] and Electric Field Conjugation (EFC, [9]), the latter of which has been used to demonstrate contrasts approaching 10^{-10} at JPL's high contrast imaging testbed (HCIT). The only thing that's critical is to make sure the region of interest is non-redundant, and then solve N wavefront control problems simultaneously with one DM. Most wavefront control algorithms, including EFC, already lend themselves naturally to solving simultaneous wavefront control problems. For example, EFC solves the problem of broadband light suppression by simultaneously solving several narrowband EFC problems (by combining narrowband "G-matrices" into a single larger matrix). In the same exact fashion, EFC and other wavefront control algorithms generalize to MSWC for 2 or more stars.

2.2.2 Sub-Nyquist Multi-Star Wavefront Control: Lab demonstrations to date

Feasibility of sub-Nyquist multi-star wavefront control was demonstrated at the Ames Coronagraph Experiment Experiment laboratory for a simple imaging system with a DM and no coronagraph, as part of our APRA-funded study. Figure 5 shows laboratory demonstrations, along with a model (albeit without wavefront errors) which shows behavior at least qualitatively very similar to the lab demonstrations. An MSWC-generalized version of the "classical speckle nulling" algorithm was used for this demonstration.

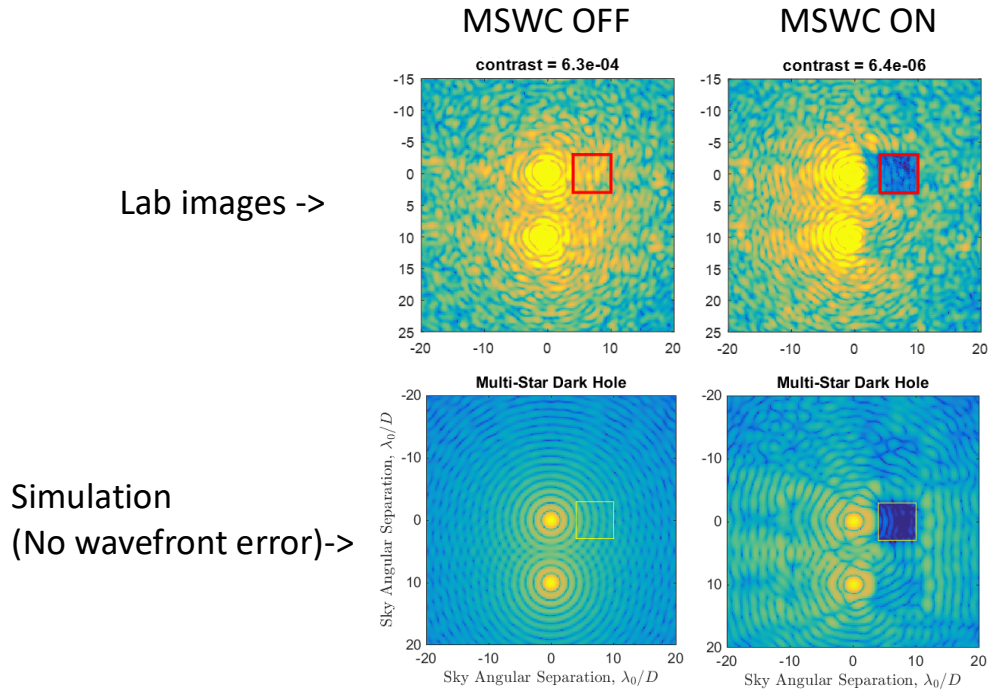

Figure 5. Laboratory demonstration of MSWC (no coronagraph). Light from each star is independently suppressed by at least a factor of 10. Contrast and size of the dark zone are likely limited by absence of coronagraph and model errors

2.2.3 Overcoming the Nyquist limit

So far, we showed (with simulations and lab experiments) that speckles can be suppressed in the presence of multiple stars as long as the region of interest lies at a sub-Nyquist separation from all stars. However, if two stars are far enough, such a region may not exist at all. In order to be able to suppress starlight from two stars that are widely separated (such as 100 λ/D or more as shown in Figure 2), we must first show that we are at least able to suppress speckles that are ~100 λ/D away from a single star. Fortunately, this appears to be possible using a technique called "Super-Nyquist Wavefront Control" [6] that we developed as part of the precursor award for this project. SNWC uses a mild grating to alias sub-Nyquist DM control modes into the super-Nyquist region. Adequate gratings are already present naturally on many DMs, such as the one we have at ACE (a 1K device made by Boston Micromachines Corporation). This "grating", sometimes called "quilting", is the print-through pattern left over from device manufacture and for some applications that require an absolutely smooth surface, it is undesirable. However, for high contrast imaging, quilting appears to be a serendipitous feature because it enables the creation of dark zones beyond the conventional outer working angle of the DM (e.g. 16 λ/D for a 32x32 DM), which until recently was generally considered to be an absolute limit.

As part of this work, we will do a trade study of the requirements on this grating and whether they are in competition with other desired characteristics on the DM. However, such a grating does not have to be integrated into the DM and can be a standalone component in the system. Furthermore, it is not necessary for the sub-Nyquist version of MSWC (i.e. MSWC-0), which already enables suppression of many interesting binary targets.

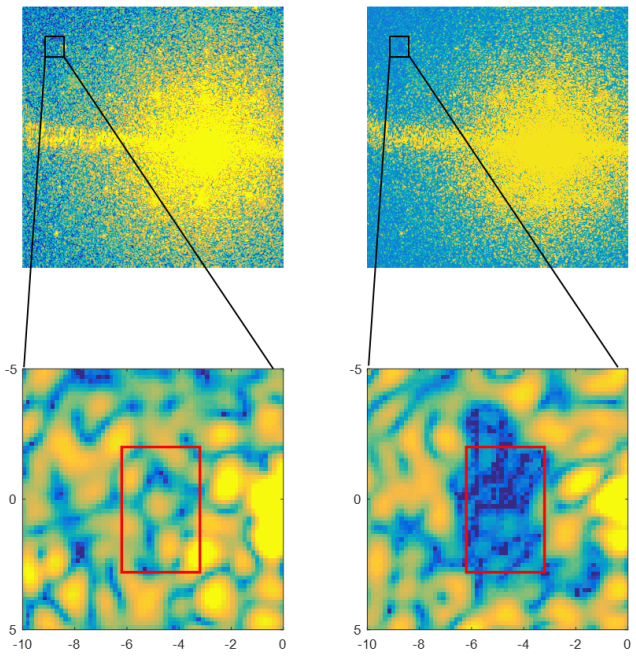

Figure 6. Laboratory demonstration of a dark zone at 100 λ/D with a 32x32 DM (with no coronagraph). Left: flat DM. Right: DM set to create a dark zone at ~100 λ/D. Suppression factor of 10 was achieved, likely limited by model errors.

Figure 6 shows a laboratory demonstration at the ACE testbed where a speckle region at 100 λ/D away from the star was suppressed by a factor of 10 (from roughly 10^{-7} to 10^{-8}) in

monochromatic light. Similarly to Figure 5, no coronagraph was used for this initial demonstration. Models also show that SNWC works in broadband light, although the size of the dark region shrinks [6, 7].

Similarly to MSWC, any conventional and mature single-star wavefront control method can be generalized to the super-Nyquist regime. What is necessary is to change the model of the system represented by wavefront control parameters (e.g. the G-matrix for EFC) so that the wavefront control treats the diffraction order nearest to the region of interest as the central star, and then performs standard (sub-Nyquist) wavefront control on it. For a lattice of DM diffraction orders, there will always be one within sub-Nyquist distance to any location in the focal plane, so a dark zone can in principle be created anywhere, as long as the energy in the diffraction order is much greater (approximately by a factor of 10) than the energy of the speckles in the region of interest.

2.2.4 Super-Nyquist Multi-Star Wavefront Control

Having the ability to create a dark zone anywhere in the focal plane allows us to generalize MSWC to super-Nyquist separations between stars. Figure 7 shows a computer demonstration of this for the case of stars separated by 70 λ/D. Although the stars are separated by a super-Nyquist distance, diffraction by the DM quilting causes a diffraction order from B to appear within the sub-Nyquist region of A, allowing sub-Nyquist MSWC to be used with respect to the original star A and the "control diffraction order" of star B. We are in the process of demonstrating super-Nyquist wavefront control in the lab and are scheduled to conclude this demonstration this year.

We also tested all these algorithms with (single-star) coronagraphs in simulation (monochromatic and broadband) and found that all versions of MSWC work with coronagraphs as well. Testing with a coronagraph is part of what we propose here.

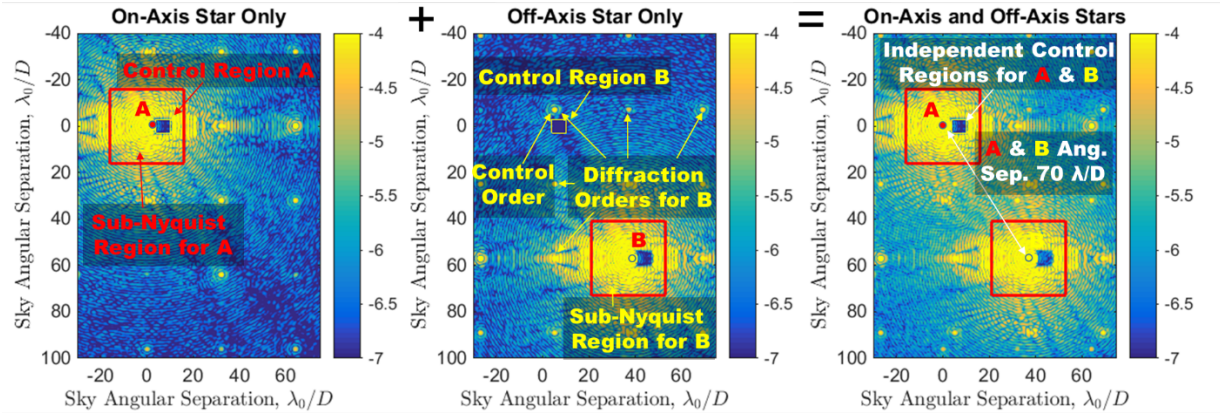

Figure 7. Diagram of super-Nyquist MSWC (MSWC-s). DM grating diffracts a "control order" of star B into a sub-Nyquist region of star A. Then, MSWC-s can be applied, treating the diffracted copy as an actual star.

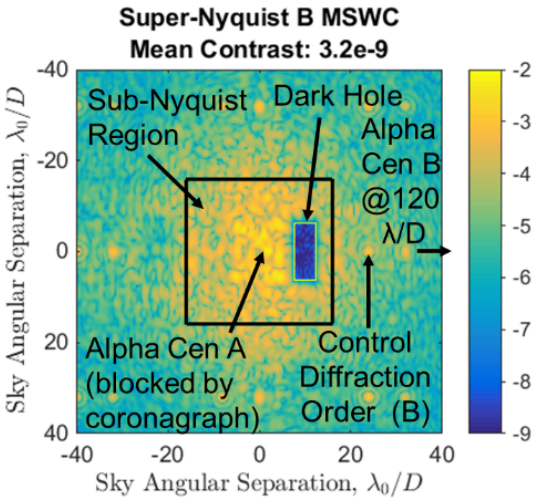

Figure 8. Simulation of super-Nyquist MSWC representative of αCen with HabEx in the 2030s. Star sepration is 120 λ/D and speckles from both stars are independently suppressed in the region of interest. (D = 4m, λ = 650nm)

3 Milestones Definition

Our work includes 3 milestones which demonstrate performance via a computer simulation, a test with a ground-based instrument, and a laboratory testbed.

Milestone 1 (Dec 31, 2018). *Computer simulation of MSWC performance applied to models of WFIRST, LUVOIR, and HabEx instruments, that is comparable to single-star performance on those missions, using designs and performance specified by mission study teams.*

Specifically,

(1) raw contrast is within a factor of 2 of official single-star performance for WFIRST, LUVOIR, HabEx, respectively (where single-star performance is specified by mission study team simulations on single-stars in STDT reports)

*(2) IWA is within 50% of official single-star performance for WFIRST, LUVOIR, and HabEx (i.e. IWA < 1.5 * IWA_single_star_performance).*

Under the following conditions:

(a) bandwidth is 10%;

(b) for aCen AB separation, delta-mag, and spectra;

(c) using coronagraph designs specified by respective mission teams (interim or final reports in case of LUVOIR and HabEx).

It is expected that the leak from aCen AB for all 3 missions will be the dominant residual after conventional single-star wavefront control, so milestone 1 represents an improvement in sensitivity on aCen AB (and similar stars) relative to the current mission baselines, and enables performance on binaries comparable to that of single stars.

In order to establish the "official single-star performance" referenced in the milestone, we will work with LUVOIR and HabEx STDTs, and the WFIRST CGI team, to obtain contrast curves that represent each mission's performance on single stars as of March 2018 (current expected date for the LUVOIR and HabEx interim reports), and then reproduce that baseline with our single-star wavefront control code as a control experiment. This will enable a more direct comparison of how MSWC performs against the single star case.

Milestone 2 (April 30, 2019). *Demonstration of MSWC with a real instrument (SCExAO), to the following performance:*

(1) 10x improvement in contrast relative to a control experiment running standard single-star wavefront control on a binary;
(2) in a dark zone region between 4 and 6 l/D relative to the on-axis star;

Under the following conditions:

(a) using an internal calibration source as the light source, and moving it to represent binaries (or two fibers, if available)
(b) in monochromatic light
(c) using separations and delta-mags corresponding to at least one real binary on the sky.

The main idea behind milestone 2 is to demonstrate that MSWC achieves an order of magnitude better contrast on binary stars with SCExAO than conventional (i.e. single-star) techniques on binaries. In addition to demonstrating a new mode on SCExAO, this will also test MSWC with a real system (albeit with a calibration source rather than the sky), demonstrating that MSWC is compatible with all the complexities of a full instrument, and preparing for an on-sky test of MSWC with SCExAO.

Milestone 3 (Dec 31, 2019). *Laboratory Demonstration of the following performance:*

(1) 1e-7 raw contrast in monochromatic light;
(2) in a region between 4 and 6 l/D;

Under the following conditions:

(a) for at least two real representative binary target where the uncorrected contrast floor from the off-axis target is 1e-6 or greater.
(b) using an aperture corresponding to at least one of: WFIRST, LUVOIR and HabEx
(c) in monochromatic light.

Notes:

- Milestones 2 and 3 are tentative and may be revised based on the results of first year's work, after conferring with the TAC and subject to TAC approval.
- As a stretch goal, we will do a systematic study of a range of separations and delta-magnitudes of binary stars to explore the efficacy of MSWC on a broader binary parameter space.
- The contrast milestone 3 is aiming for (1e-7) is based on what we expect to be able to confidently achieve limited by the ACE testbed environment. Although it is not as deep as WFIRST, LUVOIR, HabEx contrast requirements, it does represent a significant advance

in the maturity of the technology. Furthermore, it would validate models at least down to 1e-7 levels, which can then be used to predict whether MSWC can achieve deeper contrasts, and prepare it for subsequent vacuum testing (outside the scope of this work).

4 Experiment Description

4.1 Computer-based simulations and modeling

We will further develop and test computer-based models of MSWC on proposed instruments for WFIRST, LUVOIR, and HabEx, as well as on the ACE and SCExAO optical layouts. These models will be used to develop and tune MSWC to reach milestone 1 as well as to optimize the algorithms for milestone 2 and 3, and optimize the optical layout for milestone 3. We will use the official WFIRST, LUVOIR, and HabEx instrument prescription in our simulations, make sure to incorporate known important effects identified by mission study teams such as jitter, and study how tolerant MSWC is to them. For the case of WFIRST, we will also investigate whether the brightness of Alpha Centauri enables a sufficient improvement in WFIRST performance contrast to reach the sensitivity necessary for potentially habitable planets. The ARC Hyperwall Cluster computing facility will be used to rapidly simulate computation-intensive trade studies and alternative optimization methods. After achieving milestone 1, modeling efforts will continue in parallel with laboratory work to make our models properly account for all the physics and noise down to 1e-7 contrast, validate the models, and in develop the technology to the point where it is ready for vacuum testing.

4.2 Testing at the Ames Coronagraph Experiment (ACE) laboratory

Laboratory demonstrations of MSWC will be conducted at the Ames Coronagraph Experiment (ACE) laboratory. The ACE testbed is a state-of-the art facility operating in temperature-stabilized air, designed for development of coronagraph technologies and focusing on the PIAA coronagraph development. For many years, it had been pushing state of the art performance at IWAs < 2 λ/D (Figure 9) and [10] for single-star cases using the PIAA coronagraph. Over the past 2 years, it has also pioneered the development of MSWC through TRL3 (section 2.2 and [11]).

The ACE lab offers existing and proven advanced hardware which will be used for the work in this proposal:

- Fully functioning wavefront control system that includes a 32x32 Boston Micromachines Corporation (BMC) DM and an EFC algorithm that will be used as the basis for the WC algorithms described here.
- PIAA coronagraph [12] consisting of PIAA mirrors, occulting mask, as well as inverse PIAA lenses and mirrors. In addition, a parallel effort is funded to develop the PIAACMC coronagraph, which we can use with MSWC if simulations show that it performs well, complementing and synergizing with that work (and possibly enabling vacuum tests at HCIT-2 in addition to ACE tests, time permitting).
- Several light sources coupled into single-mode fibers to create star images as if they were delivered by a telescope into our instrument. These sources include several visible monochromatic lasers as well as an NKT photonics white light laser with tunable low-

and high-pass filters allowing the selection of any bandwidth with any central frequency in visible and near infrared light. The fiber is mounted on an XYZ motorized stage with very repeatable closed-loop computer-controlled positioning. This has been extensively used to simulate off-axis sources at very precise off-axis amounts. Our most commonly used laser sources also have computer-controlled variable power.

- A system to create multi-star sources for MSWC. Whenever our system is asked to take a multi-star image, it runs an automated utility that moves a high precision motorized XYZ stage to all desired star positions, takes exposures at each fiber position, and then combines them into a single image, with any desired weights on stars. The same procedure is repeated with the light off to construct a dark frame. This enables the creation of star systems with a wide range of geometries and relative star brightnesses. The motion stage is precise enough that high contrast is maintained if the fiber is moved and returned to the same nominal location. As compared to an actual two-star source, such an image will have sqrt(2) greater read noise, but in other respects should be equivalent to taking a single exposure on a two-star source. (In fact, for a low enough photon rate, one cannot distinguish between an actual binary star, or a single star switching randomly between two positions.) Furthermore, this configuration ensures that the light from the two "stars" is mutually incoherent, which is critical to ensure a proper representation of reality. On the other hand, two fiber sources next to each other may couple modes and become partially coherent, so care needs to be exercised to make sure they are incoherent. Aside from the greater read noise, we do not expect this technique to make our demonstrations either optimistic or pessimistic in terms of performance limits.
- Polarization-maintaining fibers as well as several polarizers to study polarization effects. However, studies of polarization effects are theoretically expected to impact multi-star high contrast imaging in much the same way as single star high contrast imaging, and are typically an issue for smaller inner working angles and more aggressive contrast levels than we are aiming with our milestones at our target TRL. They will be addressed in subsequent development efforts and are outside the scope of this particular effort.
- A module to enable high-precision astrometry which uses diffractive masks in the entrance pupil [13]. This module enables a very simple way to insert custom diffractive masks. Custom diffractive masks are not critical for meeting the milestones in this proposal (which can be met using the existing “grating” on the surface of the DM), but are expected to lead to better contrast and thus reduce risk.
- Modeling capability which we use to design experimental tests and predict performance as well as to diagnose potential limiting factors. We will use models extensively for this project, and validate them on experiments.

The testbed is reconfigurable with several modes that have been used before. One of the most important differences between modes is whether the Deformable Mirror is placed before or after the PIAA mirrors, and whether an inverse PIAA is used. These decisions have effects on off-axis stars that are not fully known, so we will simulate different configurations and select the one that leads to the best performance in simulations.

The ACE team has many years of experience in high contrast testing which we will bring to bear on the testing of new WC methods proposed here. Our proven test methods proceed in cycles usually consisting of: optimizing algorithms on testbed models and checking they reach desired

performance in simulation; testing algorithms on the testbed, noting any deviation from models; analyzing test data, performing targeted experiments and simulations to identify limiting factors, updating the models to include the limiting factors; and finally re-optimizing WC algorithms or hardware to eliminate limiting factors.

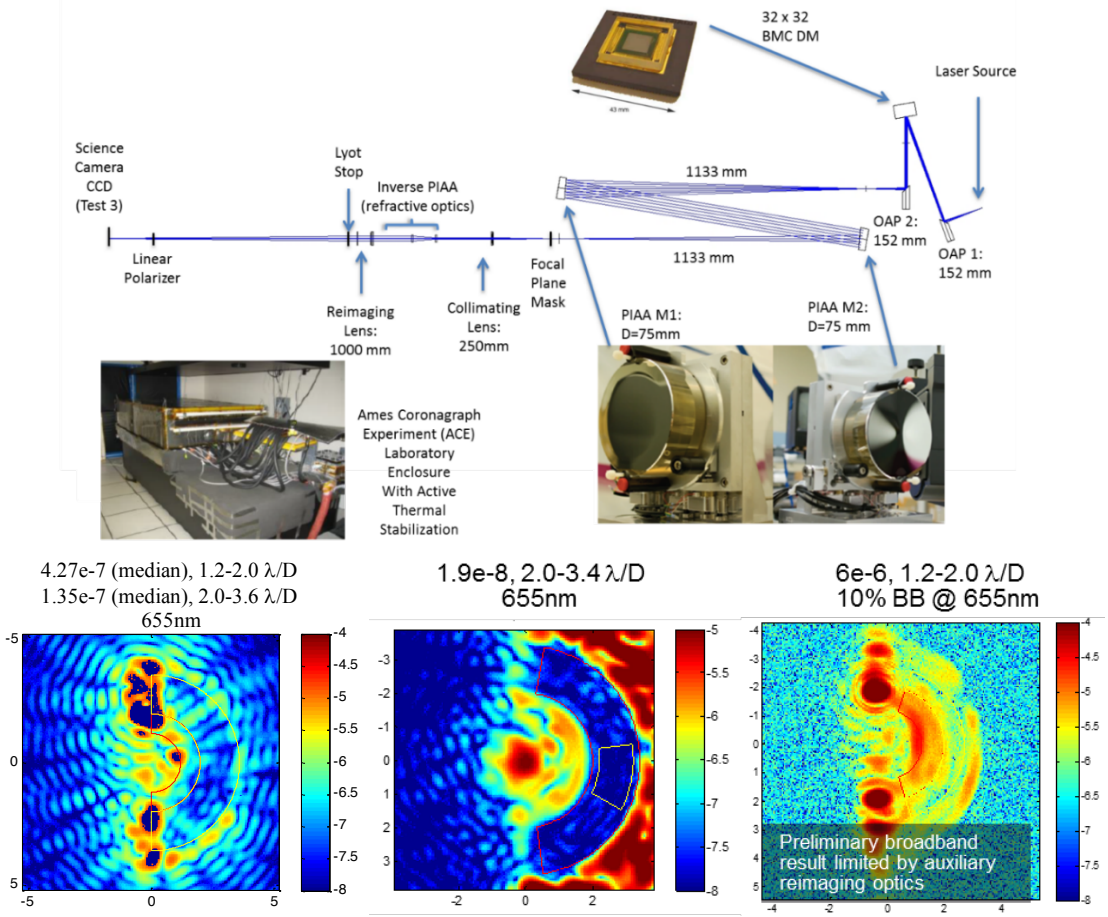

Figure 9. Top: ACE lab image and optical layout used for the results on the bottom. Bottom: High contrast demonstrations, showing, respectively, 4.3e-7 and 1.4e-7 (median) contrasts in the 1.2-2.0 λ/D and 2.0-3.6 λ/D regions at 655nm; 1.9x10^{-8} mean contrast between 2.0 and 3.4 λ/D; and 6e-6 contrast between 1.2 and 2.0 l/D in a 10%-wide band centered on 655nm (dark zones are shown by red and yellow outlines).

We are also committed to training the next generation of scientists and engineers, and welcome student interns. The ACE lab has had several successful student and postdoc projects over the past few years (e.g. [14,15]), and expect that the work described here is fertile ground for student-led spinoff projects and student participation on non-critical tasks.

4.3 Testing at SCExAO

The Subaru Coronagraphic Extreme Adaptive Optics (SCExAO) Instrument is a high contrast imager optimized for very low inner working angle (~1 λ/D) observations of faint structures such as disks and planets around their host stars. Unlike other platforms of this type, SCExAO is a testbed, which offers access to scientists to prototype and test new techniques and technologies for future high contrast imaging ground and space based instruments. We will test MSWC with

SCExAO, starting with the calibration source (during the day) and then on the sky (using time dedicated to one of the SCExAO engineering runs).

Figure 10 shows the infrared bench of the SCExAO instrument. SCExAO offers a calibration light source in the entrance focal plane of the telescope, which we will use for conducting experiments during the day. The light is first incident on a 2000 element deformable mirror that is used on-sky to improve the Strehl to the extreme AO regime, but in the laboratory is capable of being used for various forms of wavefront control. Following the DM, there is a pupil wheel that can be used to insert various masks which we will use for insertion of the segmented pupil mask to mimic the LUVOIR and HabEx primary. The photon counting SAPHIRA detector is typically used for wavefront control and we will use it for MSWC. SCExAO includes various coronagraphs including the PIAACMC, PIAA, vector vortex, 8-octant phase mask, 4-quadrant phase mask and the shaped pupil. We will baseline the PIAACMC for this proposal, but as a goal test as many coronagraphs as possible with MSWC. The CHARIS integral field spectrograph will be used to study the outcome of the focal plane wavefront control across a large band.

Calibration source:

Light is delivered to the SCExAO bench via a single endlessly single mode fiber (ESMF), which insures that the artificial star is diffraction limited from 600-2400 nm (R-K band). Within the calibration source box, light from a halogen lamp, a super continuum source, as well as various lasers can be injected into the ESMF to be delivered to the bench for the characterization of coronagraphs, and used for wavefront control. In order to create a binary star image, we will baseline the same procedure as in Section 4.2 (i.e. take two images with a single source at two different locations and add them together).

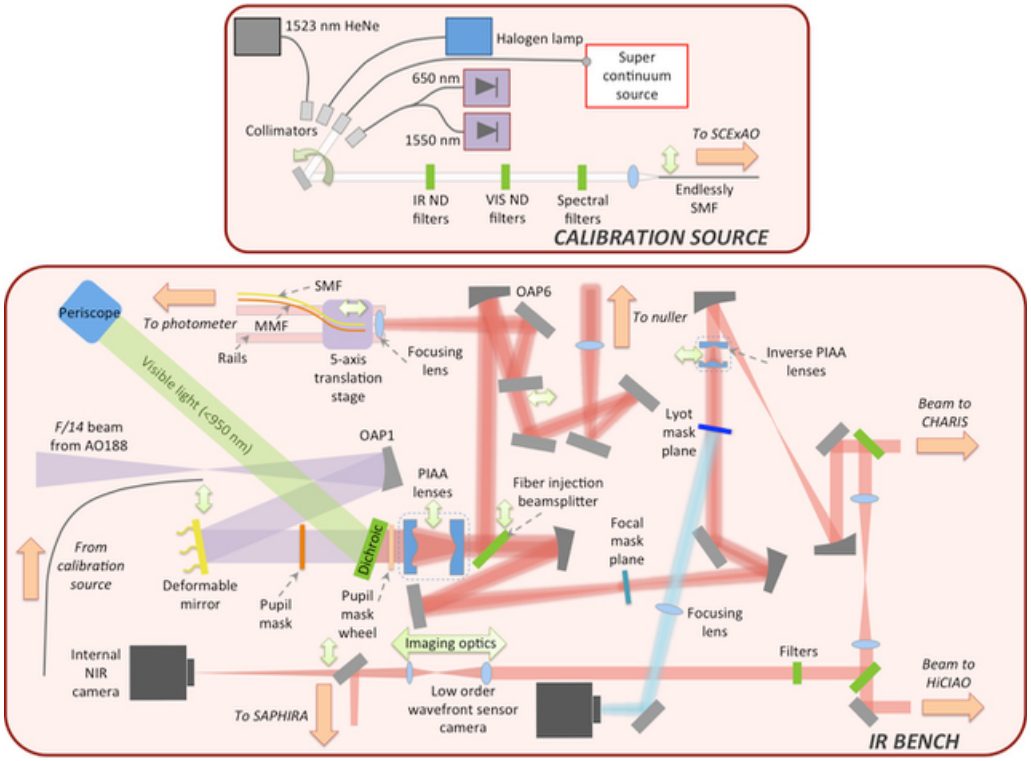

Figure 10: An illustration of the IR bench of SCExAO as well as the calibration source.

SCExAO will help mature MSWC in several respects that cannot be accomplished with a laboratory benchtop test. No matter how promising highly-controlled laboratory tests for MSWC are, the ultimate goal of MSWC is to improve direct imaging scientific capabilities of a future NASA direct imaging mission. On-sky testing of MSWC with SCExAO allows a full ``end-to-end'' system test and validation of MSWC as an efficacious method that ultimately enables improved scientific output.

The value of on-sky testing has been demonstrated over time for multiple projects. For example, Vulcan, which was the ground based test precursor of Kepler transit photometry mission which allowed to learn many features of detectors and transmission fluctuations of the atmosphere.

From a technical standpoint, recent experience demonstrates that testing new wavefront control and coronagraphy advances on sky behind an extreme AO system, specifically SCExAO, reveal information that may be hidden from laboratory predictions. For example, recent work by Currie, Kasdin, & Groff (2018, PASP in press) both the SCExAO internal source/wavefront error lab tests and real on-sky tests validated the robustness of the shaped-pupil coronagraph to low-order aberrations over a range of Strehl ratios relevant for ground-based extreme AO and future NASA missions and compared these results to those for other coronagraph architectures (S.R. ~0.57 to 0.93 to 0.99). The results were clear: while qualitatively the SPC performed as expected (low sensitivity to low-order modes), the on-sky tests revealed that the relative advantage of the SPC was larger than expected from laboratory data alone.

From a scientific standpoint, on-sky testing with SCExAO allows us to understand the gain of MSWC when integrated into a larger system architecture conducting science observations and detecting/extracting physical parameters from astrophysical objects. SCExAO observations will allow us to measure the gain in raw contrast, the stability of the speckled halo for PSF subtraction vs. other methods, and the practical gain in planet detectability and spectral extraction. All of these aspects are helpful for assessing the advantage of MSWC.

5 Data Measurement & Analysis

This section describes the details of the data measurements and analysis to reach milestones 1-3. Although milestone 1 is based on computer simulations and the other two are lab demonstrations, we are keeping our analysis and data products as similar as possible between different milestones, regardless of whether the data comes from a computer or the lab. This helps keep the simulations as relevant as possible to the lab demonstrations, allows calibrating our testbed models better, and enables testing and debugging our analysis methods on simulated data, which is more efficient. However, some calibrations described below (e.g. star brightness, plate scale) will of course be known a priori for milestone 1 because they would be specified in a configuration file read by the simulator code. These calibrations are labeled as "milestones 2 and 3 only".

5.1 Definitions

The contrast metric requires a measurement of the intensity of speckles appearing within the dark field, relative to the intensity of the incident star. In the following paragraphs we define the terms involved in this process, spell out the measurement steps, and specify the data products.

The definitions below are based on standard ones established in many previous TDEM projects, but it should be noted that a recent study by a Science Analysis Group of the ExoPAG

[16] proposed new definitions and a figure of merit called the "performance gap", which is based on fundamental concepts in signal detection theory. In order to maintain continuity with past projects, we will continue using the older established definitions for purposes of formalizing milestones and success criteria, but also explore the "performance gap" metric as time permits.

5.1.1 "Raw" Image and "Calibrated" Image (milestones 2 and 3 only)

Standard techniques for the acquisition of camera images are used. We define a "raw" image to be the 2D array of pixel values image obtained by reading the charge from each pixel of the camera detector, amplifying and sending it to an analog-to-digital converter. We define a "calibrated" image to be a raw image that has had background bias subtracted and the detector responsivity normalized by dividing by a flat-field image (if the flat field is significantly non-uniform). Saturated images are avoided by choosing appropriate settings for the exposure time, camera gain (if selectable) and source brightness in order to avoid the confusion of camera detector blooming and other potential camera detector nonlinearities. All raw images used for milestone tests are permanently archived and available for later analysis.

5.1.2 DM flat (milestones 2 and 3 only)

We define "flat" to be a DM setting in which actuators are set to a predetermined surface figure that is approximately flat (typically, about ~100V for a BMC DM, with appropriate variations to make the surface figure flat).

5.1.3 Star (milestones 2 and 3 only)

We define the "star" to be a bare single mode fiber tip, 0.22 numerical aperture with light relayed via the optical fiber from a source outside the optical enclosure wall (e.g. 650 nm frequency-stabilized laser). This "star" is the only source of light in the optical path. It is a stand-in for the star image that would have been formed by a telescope system in a focal plane immediately upstream of the coronagraph. A binary star system is created by moving this fiber to the on-axis and off-axis star locations and then adding the images as described in Sec. 4.2.

5.1.4 Wavefront control iteration.

We define "wavefront control iteration" to be a measurement of the complex-valued field in the dark zone followed by a MSWC DM correction aimed at removing coherent light in the dark zone from both stars. Such iterations will be repeated for as many cycles as are needed to reach a desired level of speckle suppression.

5.1.5 Contrast field

The "Contrast field" is a dimensionless map (2D array of numbers) representing for each pixel of the detector, the ratio of its value to the value of the peak of the central on-axis PSF that would be measured in the same conditions (camera setting, exposure time, central source illumination at the input of the instrument) if the coronagraph focal plane mask were removed. Measurement of the contrast field is detailed in sec. 5.4.

5.1.6 Contrast value

"Contrast value" is a dimensionless quantity which is the average value of the contrast field over the dark zone adopted for the experiment. Its measurement is detailed in sec. 5.5. When talking about average value of the contrast field over regions other than the dark zone, we use the term "mean contrast".

5.1.7 "Statistical Confidence" (milestones 2 and 3 only).

The measurement of coronagraph instrument contrast at levels better than the success threshold must be statistically significant, ensuring that success is not an artifact of the tails of a noise distribution. This noise, averaged over the dark zone, comprises measurement noise (read noise and shot noise) and systematic noise (photometric calibration).

The measured contrast, averaged over the dark zone, will be considered significantly better than the threshold if it is at least 3σ below the threshold contrast. If the noise were Gaussian, this would correspond to the threshold being outside of a 99.9% one-sided confidence interval about the measured contrast. The σ adopted for this criterion accommodates both the measurement noise averaged over the dark zone and calibration uncertainty. ACE typically experiences calibration uncertainties on the order of 10%, and it is straightforward to take images with measurement noise well below this level. This means that the measured contrast will have satisfied the statistical confidence requirement if the demonstrated contrast value is ~ 30% better than the contrast threshold stated in the milestone, with the actual numbers depending on more precise noise characterizations which we will do as part of this work.

It should be noted that this definition is a significant simplification of the statistical confidence criterion used in many previous TDEM projects, especially PIAA experiments on HCIT. These experiments relied on 3 sets of data with 1000 measurements each. That criterion was based on repeatability and stability constraints designed to test the environmental and wavefront control properties of the testbed. On the other hand, the experiment described here is designed to isolate the effects of the coronagraphic architecture and elements, and so does not include general testbed verification activities. Also, from experience, experiments that passed the simpler metric presented here have never failed the more complicated criterion used in the past projects.

For a successful high-contrast demonstration, the architecture-specific coronagraphic elements (PIAA mirrors, occulting mask, Lyot stop) must be properly fabricated and aligned, and in addition, the supporting equipment must all be functioning nominally -- this includes the deformable mirror, all motion control stages and actuators, the light source, the testbed thermal and vacuum environment, and all support electronics. The milestone demonstrations can be idealized as attempts to identify the limiting performance allowed by the coronagraphic components, but they are often limited by the performance of the non-coronagraphic elements. Once measurement and systematic noise have been understood and accounted for, no combination of behaviors of the non-coronagraphic elements can produce results better than the limits set by the coronagraphic elements. In this way, the best achieved performance can be interpreted as an upper limit on the ultimate performance allowed by the architecture-specific coronagraphic elements.

5.2 Measurement of the Star Brightness (milestones 2 and 3 only)

All "contrast" measurements are normalized to the intensity peak obtained when the occulter is removed and the Lyot stop is in place (unocculted star peak brightness). Because the camera

dynamic range is typically ~10^4, a so-called "photometric fiducial ladder" calibration procedure is necessary to enable measurements of contrast as low as 10^{-9}. This is done by identifying several fiducial regions in the focal plane, specifically regions a few λ/D wide consisting of speckles whose shape and contrast does not vary much during wavefront control actuation of the DM. In a typical ladder, the first fiducial region is the unocculted PSF itself, the second region can be with the occulter in or out, and having contrast of about 10^{-3}, the third region is with the occulter in, and contrast of about 10^{-6}, etc.

Mean contrast of these fiducial calibration regions is measured iteratively. Specifically, in the zeroth step, the occulter is moved out and the exposure time (and if possible, laser power) is set such that the unocculted PSF is close to saturation, but still in the linear range of the detector. Thus, contrast of each pixel in the image can be directly computed by normalizing pixel values to the peak brightness of the PSF. Mean contrast in this region 1 (PSF core) is also computed.

Then, during the *n*-th step, assume that the mean contrast of the *n*-th region is known (as with mathematical induction). An image is taken with exposure time (and if possible, laser power) set such that *n*-th and *n+1*-st regions are both seen unsaturated with high SNR on the same image, and within the linear response of the detector. The knowledge of mean contrast in the *n*-th region then allows computing the contrast of each pixel in that image as well as calibrating the mean contrast in the region *n+1*. This completes the induction and allows measurement of contrast down to any level as long as fiducial regions can be found at every step of the induction.

5.3 Measurement of the focal plane scale

The focal plane scale is defined by the displacement (pixels) of the PSF's photocenter in the absence of a focal plane mask in the system for a physical displacement of the light source by fλ/D, where f and D are respectively the focal length and diameter of beam at the input of the system (before PIAA optics). All angular separations given in this document adopt this definition. The PSF photocenter is defined as the intensity-weighted center of the PSF, and is a linear function of the source position at the input of the system. With the above definition, the focal plane scale value obtained is independent of the source offset used in the measurement. We will empirically measure the focal plane scale (both in the lab and in the simulator) by moving the light source by a known amplitude and measuring its photocenter, and verify that the obtained scale matches the value expected from the optical design of the PIAA mirrors and re-imaging optics.

5.4 Measurement of the Coronagraph Contrast Field

Each "coronagraph contrast field" (sec. 5.1.5) is obtained as follows:

1. The occulting mask is placed on the star image.

2. A long-exposure (e.g. seconds) image is taken of the coronagraph field (i.e. the suppressed star plus surrounding speckle field) with the coronagraph focal plane mask in place. A typical geometry of the dark zone is shown in Figure 9.

3. The resulting image is divided by the peak value of the on-axis reference star to produce a "contrast field" image, as discussed in Sec. 5.2.

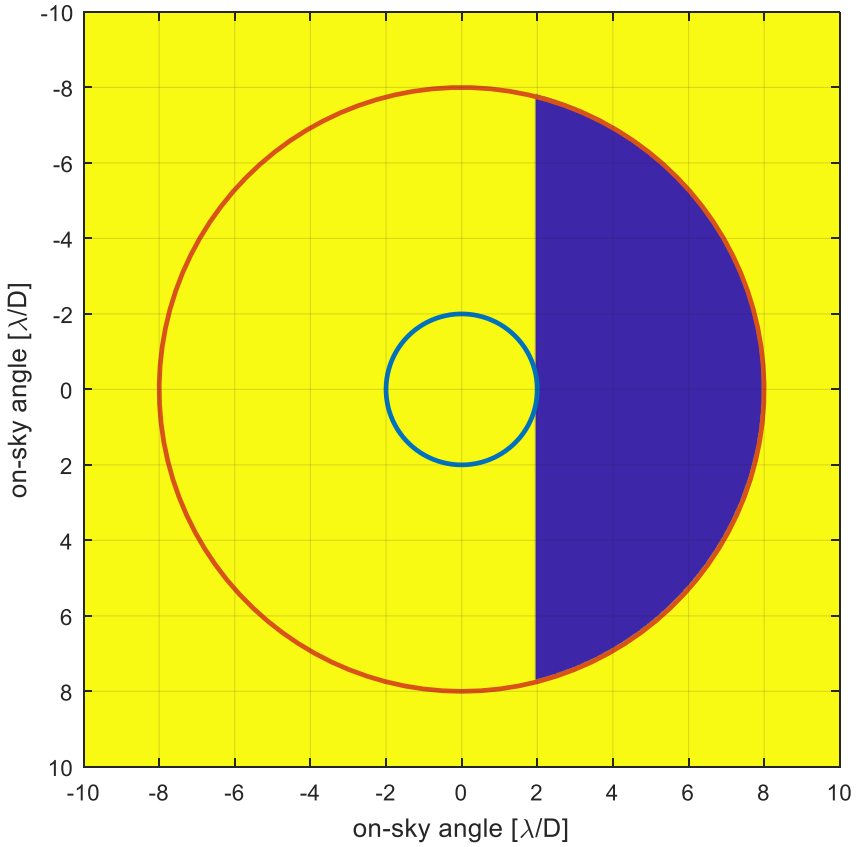

Figure 10. Dark zone geometry. The blue and red circles correspond to the inner and outer working angles, respectively. The D-shaped high contrast region, or "dark zone", is shown in blue. In this example, the dark zone is bounded by IWA = 2 λ/D and OWA = 8 λ/D. The actual values depend on the milestone and are specified in Sec. 3.

5.5 Contrast value for a single measurement

The contrast field is averaged within the dark zone (Figure 9) to yield the contrast value (Sec. 5.1.6) for a single measurement. This averaging is done over a single image (which itself may consist of a co-addition of consecutive camera frames and separate images of the on-axis and off-axis stars) with no statistical filtering other than removal of detector defects such as bad pixels and cosmic rays.

5.6 Milestone Verification Demonstration Procedure

The Milestone validation demonstration procedure is as follows:

1. The DM is set to flat (Sec. 5.1.2) with a reset of the wavefront control system software.

2. Wavefront control iterations are performed to iteratively converge to settings of the DM actuator driver voltages that give an acceptable high-contrast wavefront solution for the target dark zone. This typically takes several hours, starting from flat, if no prior information is available.

3. When contrast in the dark zone stops improving, a typical high-contrast measurement is made. This measurement is referred to as the contrast field image.

4. All images and data required by the certification data package (Sec. 5.7) are saved and archived.

5.7 Milestone Certification Data Package

The Principal Investigator will assemble a milestone certification data package for review by the Exoplanet Exploration Program and its Technology Advisory Committee. In the event of a consensus determination that the success criteria have been met, the Program will submit the findings of the TAC, together with the certification data package, to NASA HQ for official certification of milestone compliance. In the event of a disagreement between the Program and the TAC, NASA HQ will determine whether to accept the data package and certify compliance or request additional work.

The milestone certification data package will contain the following explanations, charts, and data products.

1. A narrative report, including a discussion of how each element of the milestone was met, an explanation of each image or group of images, appropriate tables and summary charts, and a narrative summary of the overall milestone achievement.

2. A description of the target(s) used (name(s) of the real target(s) we chose to emulate, star separation and delta-mag).

3. Calibrated images of the coronagraph transmittance profile.

4. Calibrated images of the data set, with appropriate numerical or color-coded or greyscale coded contrast values indicated, and with coordinate scales indicated in units of Airy distance (λ/D), all in demonstration of achieving the milestone elements.

5. A histogram of the brightness distribution of pixels in the high contrast dark field.

6. A set of contrast measurement values.

7. A description of the residual components of the residual light in the dark zone for each star: static coherent light, dynamic coherent light (due to time-variable pointing errors and wavefront changes too rapid to be fully corrected by the wavefront control loop) and incoherent light (ghosts, polarization leaks).

8. A plot of contrast vs. EFC iteration, as well as a plot showing contrast stability vs. time. This plot will have enough iterations to illustrate the statistical behavior of contrast during EFC operation as well as after it converged.

9. A step-by-step description of all data processing and analysis performed, along with source code and algorithm description. This will be provided in sufficient detail so an independent analysis of the raw data can be applied outside our team.

6 Success Criterion

Milestones 1, 2, and 3 are to be considered successfully met if the conditions specified by milestones 1, 2, and 3 (Sec. 3) are satisfied, with sufficient statistical confidence as described in Sec. 5.1.7.

7 Schedule

Our baseline work plan is diagrammed in Table 2. The full effort will take two years, starting January 1st 2018 and ending on December 31st 2019. Our work consists of three parallel synergistic tracks: algorithm development, tests with SCExAO, and high contrast laboratory testing at ACE. Each of these tracks has a milestone, and the combination of the three milestones is designed to bring MSWC to TRL4 and prepare it for subsequent tests in vacuum at HCIT (with possible follow-on work that is not yet funded).

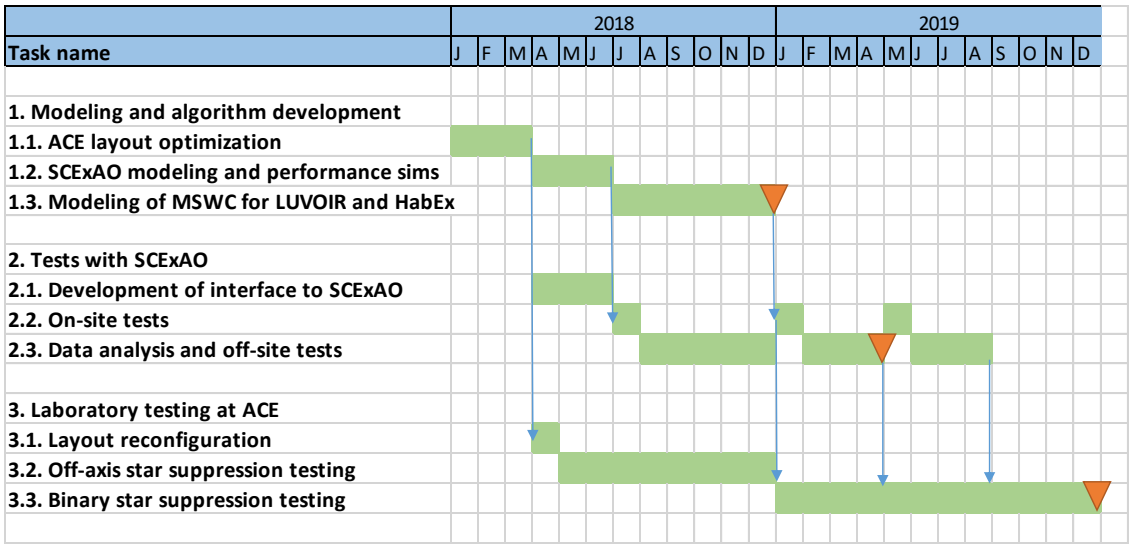

Table 2. Work Schedule diagram. The triangles are milestones 1, 2, and 3 in chronological order.

Modeling and Algorithm Development. We will start with modeling several configuration options of the PIAA coronagraph on the ACE testbed as described in section 1.2; testing MSWC with each one to ensure they are compatible with MSWC; and choosing one that achieves the best results in simulations with binary star targets from table 1. This configuration, and the MSWC algorithm with its parameters properly tuned, are then delivered to the lab in order to implement the testing part of the effort, starting April 2018. Then, the modeling effort switches to simulating MSWC with the SCExAO PIAA coronagraph (and, time permitting, the other coronagraphs in the system), and delivers a version of the algorithm with parameters tuned for SCExAO, as well as preliminary predictions of performance. Starting July 2018, the focus of the modeling effort

switches fully to testing the algorithm on instrument models of WFIRST, LUVOIR and HabEx, directly in pursuit of milestone 1, meeting it at the end of 2018. Any evolution or improvements to the algorithm enabling it to reach 10^{10} contrast with segmented apertures are flowed to SCExAO and ACE versions of the algorithm, to make sure that the hardware tests use the algorithm as close as possible to one developed for reaching the official single-star performance with WFIRST, LUVOIR, and HabEx as specified by mission teams. Modeling efforts also continue in 2019, but as part of validating hardware system tests.

Tests with SCExAO. We follow a path similar to what has been tried several times by SCExAO users and our process and schedule is based on that. We first develop a software interface to the SCExAO system based on specifications and code supplied by the SCExAO team, and ensure that our MSWC code has an interface compliant with that by June 2018. We then conduct 3 on-site tests of MSWC with SCExAO, 1-week each, with periods of at least 3 months for data analysis and off-site (remote) tests. The first two tests will be performed during the daytime with the calibration source (but otherwise with everything identical to on-sky observing), and the third test will be performed on sky using one of the regular SCExAO engineering runs. (The exact timing of the third test is uncertain, but no milestone depends on it.) The goal of the first test is to make sure that the interface works properly, to test the validity of our models, and in general to ensure basic functionality of MSWC with SCExAO. There is then a period of 5 months to adjust the models, interfaces, and MSWC code based on lessons learned, and conduct further tests remotely as necessary. The second test will then focus on performance rather than functionality and meet milestone 2 with the calibration source. The third test, which is an exploratory test without a formal milestone, will attempt to replicate milestone 2 performance on the sky. At the completion of the milestone in April 2019, we will also deliver any important aspects or lessons learned with a real instrument into the ACE testbed in order to bring it closer to reality. (Specifically, only the aspects that are likely to be shared with space instruments). These primarily include "unknown unknowns", but we do plan at least two specific deliverables represented by blue arrows in Table 2: (a) level and distribution of the speckle field caused by a larger number of optical elements and in more varied locations, than is typical for a bench-top layout; (b) understanding of requirements to make MSWC loop compatible with a real instrument interface, as well as a real instrument LOWFS loop.

We note that the schedule for SCExAO testing is shorter than the laboratory testing at ACE. This is primarily because the SCExAO milestones are much less aggressive than ACE milestones. We developed the SCExAO schedule closely with the SCExAO instrument team. The timeline is consistent with their experience for prior tests of this scale, such as a recent test of the Shaped Pupil Coronagraph.

Laboratory testing at ACE. Testing at ACE will focus on meeting of milestone 3. We start by reconfiguring to a layout deemed best by our modeling effort as described above. Then, we will focus primarily on off-axis single-star suppression for the rest of 2018, which is thought to carry the highest risk, especially in broadband light. (This risk is mitigated by existing successful broadband simulations, e.g. [6,7], which show a reduction in dark zone size with broadband, but otherwise are able to achieve deep contrasts. However, this has not been proven in the lab yet.) This process also involves a parallel modeling effort (implied in lines 3.2 and 3.3) to help diagnose limiting factors and validate models. At the end of 2018, we plan to have a system where milestone 3 can be met with either on-axis or off-axis star separately. At the beginning of 2019, we will switch our focus to testing two start simultaneously, using the latest MSWC algorithms tuned for each mission. We will reach milestone 3 at the end of 2019.

8 References and Citations

1] For latest information on HabEx and LUVOIR studies, see: https://www.jpl.nasa.gov/habex/ and https://asd.gsfc.nasa.gov/luvoir/.

2] For Exo-C and Exo-S mission concepts, see http://exep.jpl.nasa.gov/stdt/.

3] Belikov, R., Bendek, E. A., Thomas, S., J., Males, J. R., Lozi, J., "How to directly image a habitable planet around Alpha Centauri with a ~30-45cm space telescope," *Proc SPIE* 9605-41, (2015).

4] Bendek, E.A., Belikov, R., Thomas, S.J., Lozi, J., Males, J.R., "Space telescope design to directly image the habitable zone of Alpha Centauri," *Proc SPIE* 9605-40, (2015).

5] Weigert, J., Liseau, R., Thebault, P, Olofsson, G., Mora, A, Bryden, G., Marshall, J., P., Eiroa, C., Montesinos, B., Ardila, D., Augereau, J. C., Bary Aran, A., Danchi, W.C., del Burgo, C., Ertel, S., Fridlund, M.C.W., Hajigholi, M., Krivov, A.V., Pilbratt, G.L., Roberge, A., White, G.J., Wolf, S., "How dusty is alpha Centauri? Excess or non-excess over the infrared photospheres of main-sequence stars*," accepted for publication by A&A*, 2014.

6] Thomas, S., Belikov, R., Bendek, E., "Techniques for High Contrast Imaging in Multi-Star Systems I: Super-Nyquist Wavefront Control," *ApJ 810, Iss 1* (2015).

7] Sirbu, D., Thomas, S., Belikov. R. "Techniques for High Contrast Imaging in Multi-Star Systems II: Multi-Star Wavefront Control," *ApJ849*, 2 (2017).

8] Pueyo, L., Kay, J., Kasdin, N. J., McElwain, M., Groff, T., Give'on, A., Belikov, R., "Optimal Dark Hole Generation via Two Deformable Mirrors with Stroke Minimization," *Applied Optics,* Vol. 48, pp. 6296, (2009).

9] Give'on A., Belikov R., Shaklan S., and Kasdin J., "Closed loop, DM diversity-based, wavefront correction algorithm for high contrast imaging systems," *Optics Express*, Vol. 15, Iss. 19, pp. 12338-12343, 09/2007.

10] Belikov, R., Bendek, E., Greene, T.P., Guyon, O., Lozi, J., Lynch, D. H., Newman, K. E., Pluzhnik, E., Schneider, G., Tenerelli, D., Thomas, S.J., Witteborn, F. C., "EXCEDE Technology Development II: Demonstration of High Contrast at 1.2 λ/D and preliminary broadband results," *Proc SPIE 8864-31* (2013).

11] Belikov, R., Bendek, E., Pluzhnik, E., Sirbu, D., Thomas, S.J., "High contrast imaging in multi-star systems: technology development and first lab results," *Proc SPIE 9904* (2016).

12] Guyon, O., Kern, B. Belikov, R., Shaklan, S., Kuhnert, A., Give'on, A., "Phase-Induced Amplitude Apodization (PIAA) coronagraphy: recent results and future prospects," Proc SPIE 8151 (2011).

13] Bendek, E., Guyon, O., Ammons, S. M., Belikov, R., "Laboratory Demonstration of Astrometric Compensation Using a Diffractive Pupil," *PASP 125*, Iss. 932, pp. 1212-1225 (2013).

14] Newman, K., Belikov, R., Guyon, O., Balasubramanian, K., Wilson, D., "Achromatic Focal Plane Mask for Exoplanet Imaging Coronagraphy," *Proc SPIE 8864-51* (2013).

15] Bendek, E., Belikov, R., Pluzhnik, R., Guyon, O., "Compatibility of a diffractive pupil and coronagraphic imaging," *PASP 125,* Iss. 924 (2013).

16] Jensen-Clem, R., Mawet, D., Gomez Gonzalez, C.A., Absil, O., Belikov, R., Currie, T., Kenworthy, M.A., Marois, C., Mazoyer, J., Ruane, G., Tanner, A., "A New Standard for Assessing the Performance of High Contrast Imaging Systems," *accepted by ApJ* (2017).

9 List of Acronyms

ACE	Ames Coronagraph Experiment laboratory
APRA	AstroPhysics Research and Analysis
ARC	Ames Research Center
BMC	Boston Micromachines Corporation
CHARIS	Coronagraphic High Angular Resolution Integral Field Spectrograph
cpa	Cycles per Aperture
DM	Deformable Mirror
EFC	Electric Field Conjugation
ELT	Extremely Large Telescope
ESMF	Endlessly single mode fiber
Exo-C	Exoplanet Coronagraph probe mission
ExoPAG	Exoplanet Program Analysis Group
FGK	Stars of type F, G, and K
HabEx	Habitable Exoplanet Imaging Mission
HCIT	High-Contrast Imaging Testbed
HQ	Headquarters
IWA	Inner Working Angle
JPL	Jet Propulsion Laboratory
LUVOIR	Large UltraViolet / Optical / InfraRed Surveyor
MSWC	Multi-Star Wavefront Control
MSWC-0	0^{th} order, or sub-Nyquist, Multi-Star Wavefront Control
MSWC-s	Super-Nyquist Multi-Star Wavefront Control
NASA	National Aeronautics and Space Administration
PIAA	Phase Induced Amplitude Apodization
PSF	Point Spread Function
SCExAO	Subaru Coronagraphic Extreme Adaptive Optics
SIMBAD	Set of Identifications, Measurements, and Bibliography for Astronomical Data
SNR	Signal to Noise Ratio
SNWC	Super-Nyqusit Wavefront Control
STDT	Science and Technology Definition Team
TAC	Technology Assessment Committee
TDEM	Technology Development for Exoplanet Missions
TRL	Technology Readiness Level
WC	Wavefront Control
WFIRST	Wide Field InfraRed Survey Telescope